WPS1-CPR(18) 19438

E Ascasibar et al.

Overview TJ-II stellarator

Preprint of Paper to be submitted for publication in Proceeding of
27th IAEA Fusion Energy Conference

This work has been carried out within the framework of the EUROfusion Consortium and has received funding from the Euratom research and training programme 2014-2018 under grant agreement No 633053. The views and opinions expressed herein do not necessarily reflect those of the European Commission.

OVERVIEW OF TJ-II STELLARATOR RESULTS

E. Ascasíbar[1], D. Alba[1], D. Alegre[1], A. Alonso[1], J. Alonso[1], F. de Aragón[1], A. Baciero[1], J.M. Barcala[2], E. Blanco[1], J. Botija[1], L. Bueno[1], S. Cabrera[1], E. de la Cal[1], I. Calvo[1], A. Cappa[1], D. Carralero[1], R. Carrasco[1], B. Carreras[3], F. Castejón[1], R. Castro[1], A. de Castro[1], G. Catalán[1], A.A. Chmyga[4], M. Chamorro[1], A. Cooper[5], A. Dinklage[6], L. Eliseev[7], T. Estrada[1], M. Ezzat[1], F. Fernández-Marina[1], J.M. Fontdecaba[1], L. García[3], I. García-Cortés[1], R. García-Gómez[1], J. M. García-Regaña[1], A. González-Jerez[1], G. Grenfell[8], J. Guasp[1], J. Hernández-Sánchez[1], J. Hernanz[1], C. Hidalgo[1], E. Hollmann[9], A. Jiménez-Denche[1], P. Khabanov[7], N. Kharchev[10], I. Kirpitchev[1], R. Kleiber[6], A.S. Kozachek[4], L. Krupnik[4], F. Lapayese[1], M. Liniers[1], B. Liu[11], D. López-Bruna[1], A. López-Fraguas[1], B. López-Miranda[1], J. López-Rázola[1], U. Losada[1], E. de la Luna[1], A. Martín de Aguilera[1], F. Martín-Díaz[1], M. Martínez-Fuentes[1], G. Martín-Gómez[1], A.B. Martín-Rojo[1], J. Martínez-Fernández[1], K.J. McCarthy[1], F. Medina[1], M. Medrano[1], L. Melón[1], A.V. Melnikov[7], P. Méndez[1], R. Merino[1], F. J. Miguel[1], B. van Milligen[1], A. Molinero[2], B. Momo[8], P. Monreal[1], S. Mulas[1], Y. Narushima[12], M. Navarro[1], M. Ochando[1], S. Ohshima[13], J. Olivares[1], E. Oyarzábal[1], J.L. de Pablos[1], L. Pacios[1], N. Panadero[1], F. Parra[14], I. Pastor[1], A. de la Peña[1], A. Pereira[1], A.B. Portas[1], E. Poveda[1], J. A. Quintana[1], F. J. Ramos[1], G.A. Rattá[1], M. Redondo[1], E. Rincón[1], L. Ríos[1], C. Rodríguez-Fernández[1], L. Rodríguez-Rodrigo[1], B. Rojo[1], A. Ros[1], E. Rosa[1], E. Sánchez[1], J. Sánchez[1], M. Sánchez[1], E. Sánchez-Sarabia[1], S. Satake[12], J.A. Sebastián[1], R. Sharma[15], C. Silva[15], E.R. Solano[1], A. Soleto[1], B.J. Sun[1], F.L. Tabarés[1], D. Tafalla[1], H. Takahashi[12], N. Tamura[12], A. Tolkachev[1], J. Vega[1], G. Velasco[1], J.L. Velasco[1], S. Yamamoto[13] and B. Zurro and the TJ-Team[1]

[1]National Fusion Laboratory, CIEMAT, Madrid, Spain
[2]Department of Technology, CIEMAT, Madrid, Spain
[3]Universidad Carlos III, Madrid, Spain
[4]Institute of Plasma Physics, NSC KIPT Kharkov, Ukraine
[5]Swiss Alps Fusion Energy (SAFE), Vers l'Eglise, Switzerland
[6]Max-Planck-Institut für Plasmaphysik, Greifswald, Germany
[7]National Research Centre 'Kurchatov Institute', Moscow, Russian Federation
[8]Consorzio RFX (CNR, ENEA, INFN, Universitá di Padova, Acciaierie Venete SpA), Padova, Italy
[9]University of California-San Diego, San Diego, CA, United States
[10]General Physics Institute, Russian Academy of Sciences, Moscow, Russian Federation
[11]ENN Energy Research Institute, Langfang, Hebei, China
[12]National Institute for Fusion Science, Toki, Japan
[13]Institute of Advanced Energy, Kyoto University, Uji, Japan
[14]Rudolf Peierls Centre for Theoretical Physics, University of Oxford, United Kingdom
[15]IPFN, Instituto Superior Técnico, Universidade de Lisboa, Lisboa, Portugal

Email contact main author: enrique.ascasibar@ciemat.es

Abstract: The main results obtained in the TJ-II stellarator in the last two years are reported. The most important topics investigated have been: modelling and validation of impurity transport, validation of gyrokinetic simulations, turbulence characterisation, effect of magnetic configuration on transport, fuelling with pellet injection, fast particles and liquid metal PFCs.

1. INTRODUCTION

The TJ-II stellarator (heliac type, major radius 1.5 m, minor radius $\leq$ 0.22 m, four periods, average magnetic field on axis 0.95 T, plasma volume $\leq$ 1 m^3), is entering its third decade of operation. Both ECRH (two gyrotrons, 53.2 GHz, P $\leq$ 300 kW each, suitable for X2 heating) and NBI (two H^0 injectors, E $\leq$ 30 kV, P $\leq$ 600 kW each) heating methods can be used to produce and sustain the discharge. Plasma physics

research in TJ-II is focused on some selected areas posing fundamental problems that must be solved in the development of reactor-grade magnetic confinement devices, namely: impurity accumulation in stellarators, turbulence, effects of the magnetic configuration on transport in stellarators, plasma core fuelling with pellet injection, fast particle driven modes, power exhaust physics and technology, among others. The very wide range of configuration flexibility of the device (edge rotational can be varied from 1.0 to 2.2) and its rather complete set of advanced diagnostics have been instrumental for the plasma research done so far by the TJ-II team. In recent years, a substantial effort has been done by the team in strengthening its modelling capability in order to tackle the validation of theory in the areas of transport, turbulence, magnetic topology, electric fields, fast particles and the relations among them. Whenever feasible the modelling results have been extended to the largest world class stellarator/heliotrons in operation, namely LHD and W7-X. It must be noted that work done on TJ-II is relevant for both W7-X and LHD. This paper reports the main results obtained in the last two years and is organised along the list of topics mentioned in the abstract, each section covering one of them.

2. NEOCLASSICAL IMPURITY TRANSPORT

Impurity accumulation is one of the main problems that limit the plasma performance via increased radiative losses and plasma dilution. For stellarator reactor-relevant conditions, accumulation is explained as due to the negative (inwards pointing) radial electric field required to satisfy the ambipolarity constraint on the neoclassical particle fluxes. But there are some experimental observations of outward impurity flux not well understood in stellarators [1, 2] that call for improvements of the neoclassical theory. In this context a number of working lines exploring several recently discovered effects are being developed.

- Effect of tangential drifts on stellarator neoclassical transport and discussion on the solutions for φ_1 in low collisionality regimes .

Two important ingredients have often been neglected in standard neoclassical theory and simulations of stellarator plasmas. First, the component of the electrostatic potential that is non-constant along the flux surface, that we denote by φ_1. Only recently has it been acknowledged that φ_1 can affect radial impurity transport via the radial $E \times B$ advection of the variations of impurity density along the flux surfaces, which has triggered the interest in its calculation. The computation of φ_1 has been included in some modern neoclassical codes, but the number of simulations in which φ_1 has been calculated is still scarce [3]. The systematic analytical description of φ_1 has received little consideration as well. The second ingredient that has often been missing in stellarator neoclassical calculations is the component of the magnetic drift that is tangent to the flux surface, whose effect is essential to correctly determine the radial neoclassical fluxes of the bulk ions at low collisionality and small radial electric field values.

In reference [4], low collisionality neoclassical equations that include φ_1 and the tangential magnetic drift have been rigorously derived for sufficiently optimized stellarators, and the radial neoclassical fluxes for the main ions have been computed in the $1/\nu$, $\sqrt{\nu}$ and superbanana-plateau regimes. Besides, it has been proven that φ_1 can become especially large in plasma regimes in which the tangential magnetic drift counts. Therefore, the two ingredients mentioned above must be simultaneously and consistently treated, in general. The orbit averaged code KNOSOS (KiNetic Orbit-averaging-SOlver for Stellarators) has been developed, that solves the equations derived in [4].

In reference [5], a thorough analysis of the solutions for φ_1 in the $1/\nu$, $\sqrt{\nu}$ and superbanana-plateau regimes has been presented. The different asymptotic regimes for φ_1 have been identified analytically and verified with KNOSOS.

- Effect of tangential magnetic drifts on the calculation of φ_1 for realistic stellarator plasmas: LHD stellarator.

Reference [5] used academic configurations and plasma profiles in order to illustrate the different neoclassical regimes. In reference [6], it has been proven that the tangential magnetic drift is also relevant for the calculation of φ_1 in realistic stellarator plasmas. We have chosen, for the Large Helical Device, LHD, two different scenarios: medium density [7] and low density with very high ion temperature. The latter present a especially small negative radial electric field [8], a situation in which the contribution of the superbanana-plateau regime to bulk ion transport is expected to be largest. The numerical calculations have been done with the code KNOSOS following [4] (although it has to be kept in mind that the magnetic field cannot be accurately split into an optimized part and a small deviation from perfect optimization), and the results for the high-temperature plasma are shown in Fig. 1. On the left, it is depicted a calculation in which the tangential magnetic drift is artificially switched off. On the right, it can be observed that the calculation that keeps the tangential magnetic drift yields a quite larger φ_1, with a different phase. These phase differences are likely to have a strong impact on the impurity transport driven by tangential electric fields, a matter that will be discussed later in the paper. Experiments have been planned for the incoming deuterium campaigns of LHD [9] in order to validate these predictions.

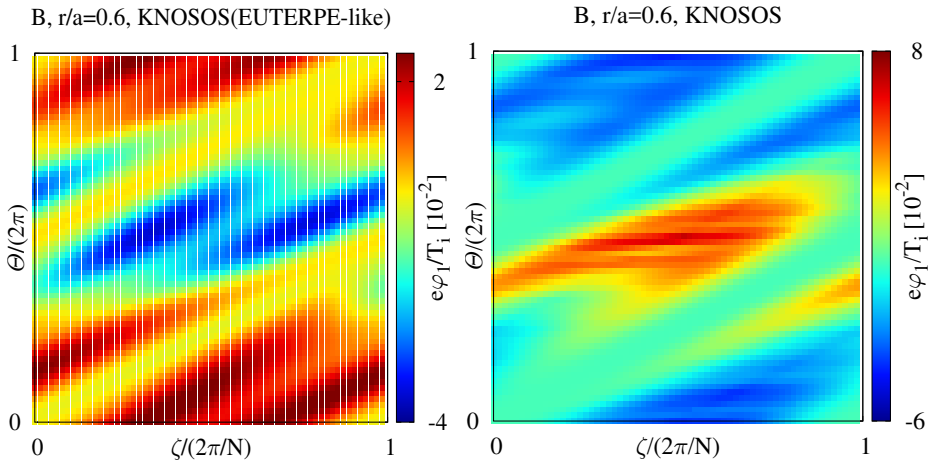

FIG. 1: Calculations of φ_1 with the KNOSOS code. Left: with the tangential magnetic drift artificially switched off. Right: keeping the tangential magnetic drift .

- Impurity flux driven by electric fields tangent to magnetic surfaces in stellarators.

The standard argument to explain the accumulation of impurities with $Z \gg 1$ relies on the, in principle, large inward pinch in the neoclassical radial impurity flux, Γ_z, caused by the typically negative stellarator radial electric field E_r. This argument was proven to be flawed, at least in some important cases, in [10], where it was shown that, if the main ions have low collisionality and the impurities are collisional, then Γ_z does not depend on

E_r. This result was interpreted in a positive way because it diminished the prevalence of E_r in Γ_z and made "temperature screening" (that is, the reduction or absence of impurity accumulation thanks to the contribution of the temperature gradient to Γ_z) more likely than previously thought.

In [10], the effect of φ_1 on Γ_z was not included. In [11], we give an analytical calculation of Γ_z for low collisionality main ions and collisional impurities, incorporating the effect of φ_1. We show that this effect can be very strong for $Z \gg 1$ and that, once it is taken into account, the dependence of Γ_z on E_r reappears. In addition, we prove that such an effect is stellarator specific (i.e., Γ_z in a tokamak does not depend on E_r, whatever φ_1). A careful analysis of the final expression for Γ_z in stellarators (that reduces to the expression derived in [10] when φ_1 vanishes) reveals that the impact of φ_1 starts to be important for φ_1 surprisingly small, $e|\varphi_1|)/T$=O(ϵ^2), where ϵ is the inverse aspect ratio. Our analytical results have been applied to the calculation of the neoclassical particle flux Γ_z versus E_r, for three charge states of tungsten in an LHD plasma (see [11]). The computation of φ_1 has been carried out with the code EUTERPE. The results show a large difference in the neoclassical impurity flux obtained with and without φ_1, and a strong dependence of the flux on E_r when φ_1 is included. Although the effect of φ_1 is typically to increase impurity accumulation, there is a small region in parameter space where its inclusion leads to impurity expulsion.

- Experimental validation with Doppler reflectometry (DR) of the variation of the radial electric field on the flux surface in electron-root stellarator plasmas.

The interest in the role of the electric field tangent to the surface on the transport of impurities, commented in the first bullet above, has dealt in most cases with ion-root plasmas, whereas electron root conditions have been barely investigated.

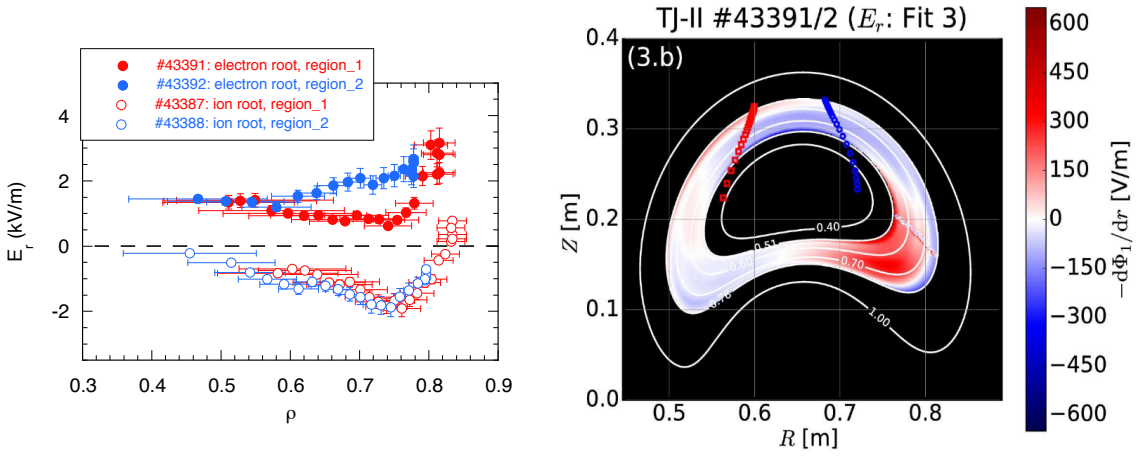

FIG. 2: Left, E_r profiles measured by the Dopppler reflectometer at turbulence scales $k_\perp \sim 6-8$ cm^{-1}, in the two plasma regions (1 in red and 2 in blue) in both electron and ion root regimes. Right, calculated contribution to the radial electric field component that arises from the radial dependency of φ_1. Plasma regions 1 and 2 are indicated by consistently coloured thick lines in the upper (external) part of the plasma cross section.

On the other hand, since φ_1, the part of the electrostatic potential that leads to the electric field tangent to the surface, depends parametrically on the flux surface label as

well, it can cause variations of the total radial electric over the flux surface. These two elements of the problem have been recently addressed [12] motivated by the observation of strong differences in the total radial electric field measured at different points over the same flux surface with DR in TJ-II electron-root plasmas, see Fig. 2, left. In Fig. 2, right, we show the calculated contribution to the radial electric field component that arises from the radial dependency of φ_1 for a TJ-II electron-root plasma (shots 43391 and 43392). Although the agreement at the specific DR measurement positions has not been quantitatively captured by the numerical simulations performed with the code EUTERPE (see ref. [12] for details), the fact that those differences occur in electron-root conditions and are practically absent under ion-root has been well reproduced by the simulations.

Motivated by the fact of having similar DR systems installed in W7-X, a plasma presenting Core Electron Root Confinement (CERC) conditions, produced in the first W7-X campaign, has been also considered for carrying out a similar analysis. In particular a high mirror configuration has been chosen due to its higher ripple in comparison with the standard configuration used in our previous work [3] and due to its higher likeliness to exhibit large φ_1 values and related effects. The results obtained, see Fig. 3, show that the region of the core in electron-root (inside r/a=0.6 approx.) shows considerably larger φ_1 amplitude than the region in ion root, which can lead to large radial electric field differences over flux surfaces in the vicinity of the root transition. The calculation with either adiabatic or kinetic electrons confirms the need of using the latter for an accurate calculation of φ_1, which, as shown in other works [13], can be larger than previously estimated in W7-X [3].

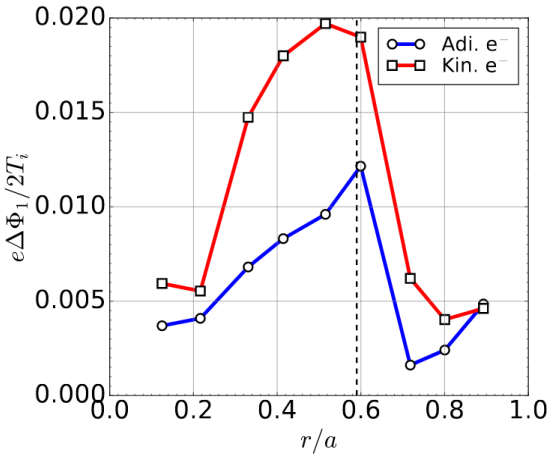

FIG. 3: EUTERPE calculation (with kinetic (red) and adiabatic (blue) electrons) of the normalized maximum variation of φ_1 over several flux surfaces of a high ripple W7-X configuration in CERC plasma conditions. The dashed line indicates approximately the region where the root change takes place

.

3. EXPERIMENTAL VALIDATION OF GLOBAL GYROKINETIC SIMULATIONS

ZFs are recognized as an important mechanism for the self regulation of plasma turbulence. Besides, the appropriate framework to study plasma turbulence is the gyrokinetic

formalism, in which kinetic simulations are affordable using appropriate codes and supercomputers. However, these codes should be carefully validated against experiment in order to be reliable. Scale resolved turbulence measurements are important to validate the simulations and to identify the type of turbulence at work. Some topics in both areas have been simulated and experimentally validated in TJ-II.

- Comparison between measurements of zonal flow relaxation in pellet-induced fast transients and gyrokinetic simulations.

Linear ZF relaxation in stellarator geometries has been studied from different perspectives. From the analytical point of view, the long term relaxation of zonal potential perturbations has been studied as an initial value problem in [14] and expressions for the frequency of the Low Frequency Oscillation (LFO), characteristic of stellarators [15], were derived. Semianalytical predictions were compared to results of numerical simulations carried out with the gyrokinetic codes GENE [16] and EUTERPE [17] in different stellarators (TJ-II, W7-X and LHD). Good agreement has been found between analytical estimations of the ZF oscillation frequency and the results from numerical simulations. This cross-benchmark has allowed not only testing the analytical calculations but also verifying the codes in this setting.

During pellet injection experiments in TJ-II [18, 19], a sudden global perturbation to the plasma potential was detected at the radial location of pellet ablation which undergoes a fast oscillatory relaxation, see Fig. 4, left.

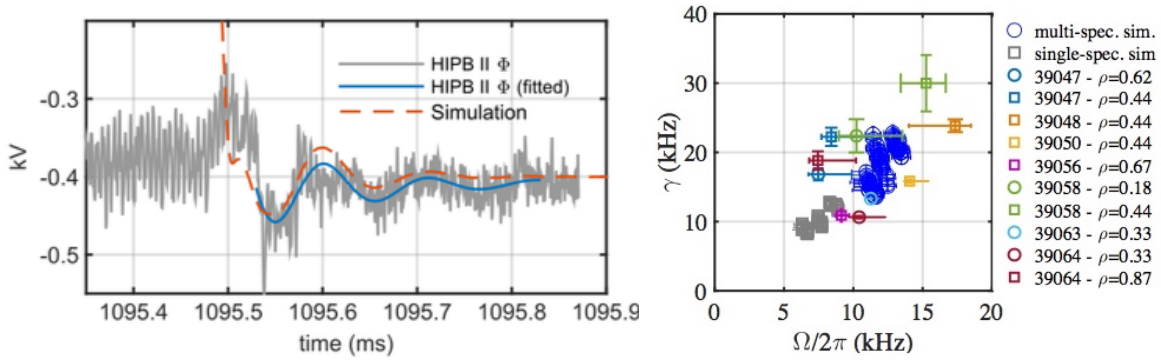

FIG. 4: Left: Comparison of a potential relaxation experimentally measured by the HIBP diagnostic in plasma discharge 39056 [20] and the numerically simulated relaxation. The figure is from [20]. Right: Damping rate (γ) vs oscillation frequency (Ω) for the experimental oscillations detected in [20]. Data are shown for the specified TJ-II discharges and for numerical simulations, both with a single (gray squares) and with multiple kinetic species (blue circles), namely, ions + electrons + C^{4+} impurity ions [21].

This phenomenon was studied numerically in global linear gyrokinetic simulations with the code EUTERPE, using the experimental plasma profiles as input for the simulations [20]. This constituted the first experimental observation of the LFO predicted analytically in [15]. The numerical simulations of oscillation frequency and damping rate of the potential oscillations reproduced qualitatively the experimental oscillations, although a quantitative agreement was not found in the first single-species simulations. In a second step, the ZF relaxation has been studied numerically in a multi-species plasma with TJ-II configurations [21]. Multi-species collisional simulations carried out with the experimental

plasma profiles from the pellet injection experiments previously analyzed in [20] showed an improved quantitative agreement in frequency and damping rate between experiment and simulations [21], as shown in Fig. 4, right.

- Validation of gyrokinetic simulations with density fluctuations spectra measured by Doppler reflectometry.

Global gyrokinetic simulations of electrostatic microinstabilities have been carried out with the EUTERPE code [22] and validated with dedicated experiments carried out during the 2017 experimental campaign in TJ-II [23]. The Doppler reflectometry (DR) system provides information on the density fluctuation wave-number spectra as well as the radial electric field and is used as the basic diagnostic for the characterisation of the plasma edge turbulence. Several ECRH scenarios have been studied in which plasma profiles are modified by changing the heating power and deposition location. Measurements have been compared to numerical simulations in which the experimental plasma profiles are used as input for the simulations.

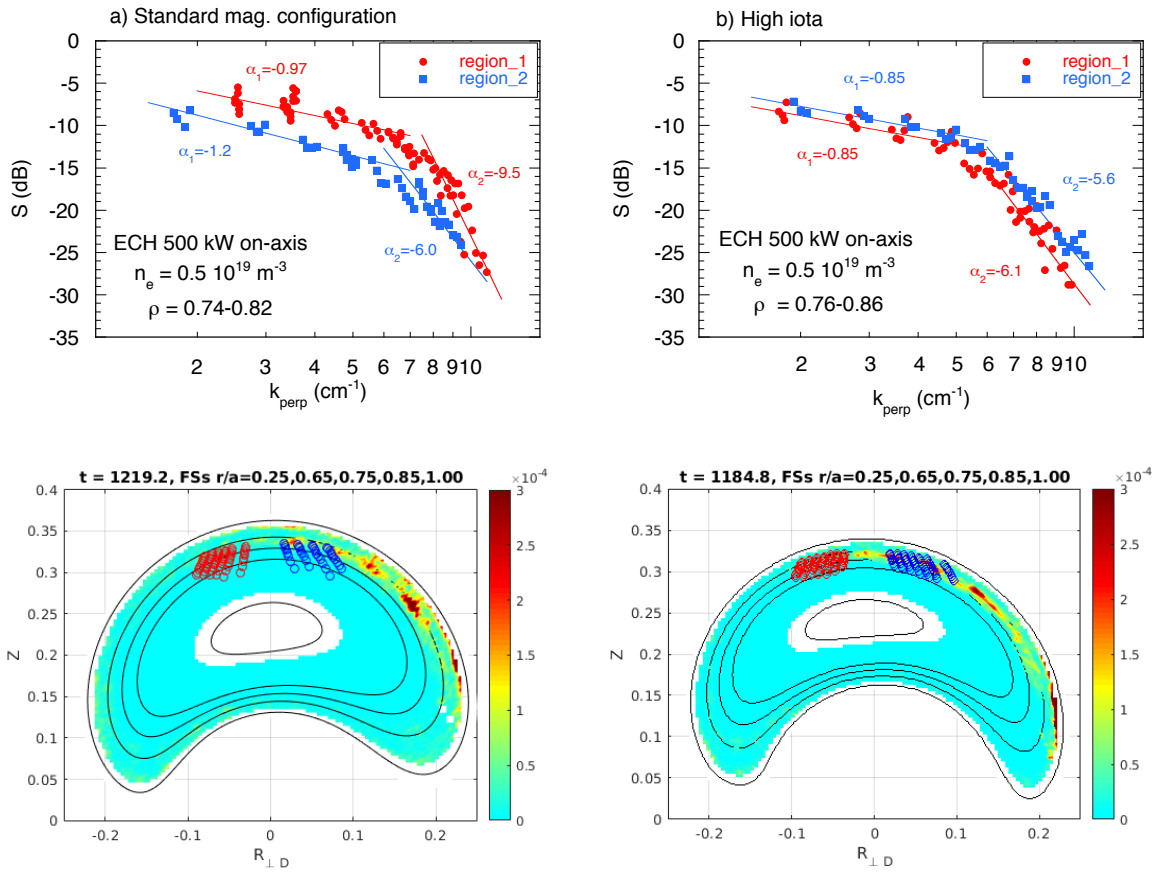

FIG. 5: Upper row: Experimental $k_\perp$ spectra measured in two plasma regions poloidally separated (see FIG. 1 caption for the explanation of regions) in the standard (left) and high iota (right) magnetic configurations. Lower row: EUTERPE simulation of the localization of the instabilities for the standard (left) and high iota (right) magnetic configurations.

Electron-driven modes, which are compatible with Trapped Electron Modes (TEM), were found unstable in the plasma edge region in linear simulations. The range of unstable

wave-numbers and the radial location of maximum instability found in simulations are consistent with the relevant wave-numbers and the radial variation of experimental density fluctuations spectra measured by the DR system. Experiments were carried out both with hydrogen and deuterium as base gas, finding no dependency of the power spectra with the bulk ion mass. In agreement with the experiment, simulations with hydrogen and deuterium show very similar results in respect to the radial location of instabilities and unstable wave-numbers, which is consistent with the electron-driven character of the unstable modes found in the simulations. The instabilities are localised toroidal and poloidally in simulations, the location of maximum instability being affected by the rotational transform. A systematic difference is found between the density fluctuation spectra measured by the DR system at poloidally separated positions on the same flux-surface. As in the case of simulations, the poloidal asymmetry of the fluctuation spectra measured by the DR system is also largely affected by the rotational transform. As an example, Fig. 5 shows in the upper row the perpendicular wavenumber spectra measured at the two poloidally separated plasma regions in the standard and high iota magnetic configurations. An asymmetry is clearly observed in the intensity of the density fluctuations in the whole $k_\perp$ range. In the standard magnetic configuration, higher turbulence level is measured in region 1 as compared with that measured in region 2, see Fig. 5, left. This asymmetry reverses in the high iota configuration, see Fig. 5, right. The lower row of Fig. 5 shows the poloidal localization of instabilities found by the EUTERPE gyrokinetic simulations. Model and experiment are in qualitative agreement: a clear poloidal asymmetry which depends on the magnetic configuration is found. But measured and simulated asymmetries have opposite phase in the standard magnetic configuration case.

- First measurements of density fluctuations in both positive and negative density gradient regions of the plasma.

A crucial open issue for next step devices and the fusion reactor is how to achieve particle fuelling in the core plasma in order to replenish the fused nuclei. Pellet fuelling systems designed to inject particles at high speed deep into the plasma are one of the main tools to achieve that goal. However, at reactor relevant plasma densities and temperatures, pellets will hardly be able to reach the core plasma region because pellet ablation will take place in the plasma edge causing plasma bumps with positive and negative density gradient regions [24, 25]. Eventually particles could be transported radially inwards by turbulence. Fluid and gyrokinetic simulations have been used to investigate the level of inward turbulent particle transport in the inverted density gradient region[26, 27] but comparison of simulations with experimental fluctuation levels and fluxes is still missing. First 2-D poloidal contour plots of plasma potential and density fluctuations have been measured with the TJ-II HIBP diagnostic [28], which have allowed to characterise turbulence in positive and negative gradient regions: density fluctuations appear both at the positive and negative gradient regions, their amplitude being minimum in the zero density gradient zone while is stronger in the negative than in the positive gradient region [29]. Gyrokinetic simulations (EUTERPE) of ion and electron-driven modes in ECRH plasmas yield results consistent with the experiment. In the electron root scenario (positive radial electric field) Ion Temperature Gradient (ITG) modes are found to be stable due to the nearly flat ion temperature profiles. Linear and collisionless Trapped Electron Modes (TEM) simulations (kinetic ions and electrons) show that the most unstable modes are located in the negative density gradient region [30].

4. INTERPLAY BETWEEN RADIAL ELECTRIC FIELDS, TURBULENCE AND ATOMIC PHYSICS

A number of research areas related to plasma turbulence in TJ-II, mainly of experimental nature so far, are providing additional valuable results.

- Impact of the edge neutral density fluctuations on the observed turbulent structures.

An almost unexplored area of research, the impact of neutral fluctuations on the observed turbulent structures has been investigated in TJ-II, showing that thermal neutrals react to low frequency plasma fluctuations [31], becoming also turbulent. Hence, neutral-induced non-linearities would be expected in plasma turbulence. The non-linear behaviour of plasma turbulence in the temperature range where ionization strongly depends on electron temperature is under investigation [32].

- L-H transition triggered by turbulence stabilization due to both zero and low-frequency varying large scale flows.

Mean radial electric fields as well as low frequency ZF-like global oscillations have been identified during the Low to High (L-H) transition in hydrogen and deuterium plasmas. No evidence of isotope effect has been observed in the L-H transition dynamics [33]. These observations emphasize the critical role of both zero and low frequency varying large-scale flows for stabilising turbulence during the triggering of the L-H transition in magnetically confined toroidal plasmas.

- Impact of the radial electric fields on turbulence spreading in the edge and Scrape-Off Layer.

Understanding filamentary and blob transport across the Scrape-Off-Layer (SOL) is a key issue for the design and operation of future devices as it is crucial in determining the power load to the divertor and first wall of the machine. Consequently, clarifying whether the SOL width is set by local effects inside the SOL region or/and by transport arriving from the plasma edge, and the role played by $E_r \times B$ sheared flows in edge-SOL coupling are important issues. The radial transport (spreading) of turbulent energy is a consequence of the redistribution of fluctuation energy from unstable regions with dominant free energy sources to adjacent regions without or with weaker free energy sources. The spreading of turbulence therefore involves transport from strongly driven (i.e., unstable) to weakly driven regions [34, 35]. Flow shear can "block" turbulence spreading, decoupling turbulence radially [36, 37]. The influence of radial electric fields on turbulence spreading has been studied experimentally in TJ-II co-NBI heated plasmas ($P_{NBI} \approx 500kW$) [**?**]. A 2-D Langmuir probe array [39] was used to measure the floating potential, ion saturation current and turbulent driven particle transport, neglecting the influence of electron temperature fluctuations. The radial electric field has been modified with the aid of a biasing electrode inserted into the plasma edge. The influence of edge biasing on plasma profiles is shown in Fig. 6. During the negative biasing phase [-300 V], the floating potential becomes more negative (Fig. 6b) and the perpendicular phase velocity increases up to 9 km/s. The latter directly reflects changes in radial electric fields induced by edge biasing. Also in this phase, the edge floating potential (Fig. 6b) and ion saturation current (Fig. 6c) profiles get steeper, while the turbulent particle flux

(Fig. 6d) is reduced in the region between the las closed flux surface (LCFS) and the far SOL, concomitant with a reduction in the magnitude of the shoulder in the ion saturation current. Thus, when the $E_r \times B$ sheared flows achieve velocity gradients comparable to the inverse of the turbulence correlation time, they affect the level of turbulence spreading and edge-SOL coupling [38]. Hence, the shearing rate of edge radial electric fields can be an important tool to suppress turbulence and decouple edge and SOL regions.

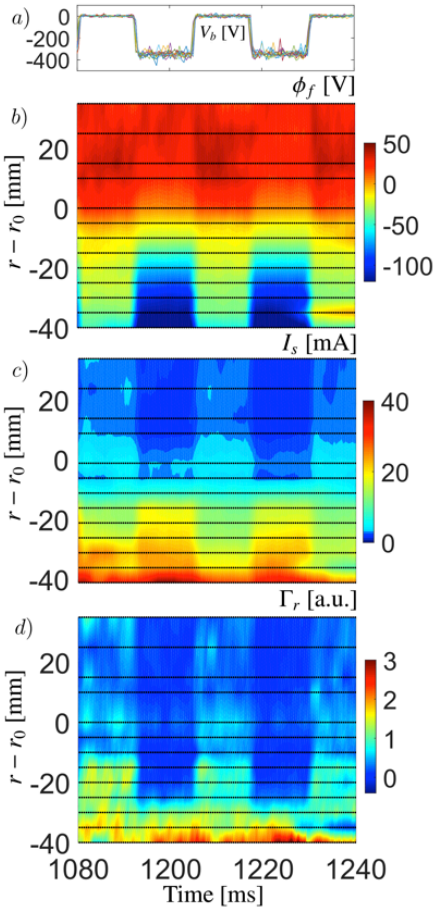

FIG. 6: a) Biasing voltage waveform; b), c) and d) Radial profiles of floating potential, ion saturation current and turbulent flux, respectively, during dynamical biasing in the plasma boundary region. r_0 denotes the location of the LCFS.

5. EFFECT OF MAGNETIC CONFIGURATION ON TRANSPORT

Transport studies in TJ-II , as in many other devices, require the consideration of magnetic configurations where magnetic islands can be present. These are often detected as coherent modes in magnetic signals where, owing to the low poloidal mode numbers of the main low-order rationals of the rotational transform, the helicity can be resolved with the help of a poloidal array of magnetic coils or other diagnostics with some degree of poloidal/toroidal resolution. Since 1D transport codes are well-developed tools for transport analyses, a practical transformation of coordinates has been developed [40] to adapt the metric coefficients of an unperturbed configuration to a new one where the islands (or stochastic) region is excluded. Such regions can always be calculated separately if transport is non-trivial in them. This result is illustrated by Fig. 7. It shows that the analytical

model developed in [40] yields values of the metric coefficients for a perturbed magnetic configuration that are in excellent agreement with the ones obtained numerically from the Poincare sections. It constitutes a very practical solution to perform 1-D transport in configurations with magnetic islands, where the islands width or location change.

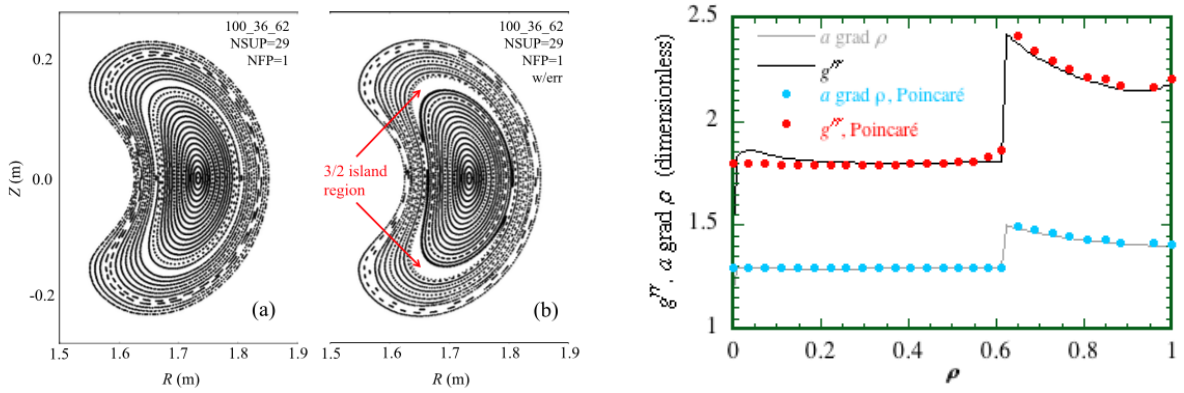

FIG. 7: Left: A TJ-II magnetic configuration perturbed by a small error field. Right: Excellent agreement between the metric coefficients calculated numerically and the ones obtained from the analytical model developed in [40]

In addition, it is often the case that the MHD modes associated to low order rationals of the rotational transform do not respect the four-fold toroidal periodicity of TJ-II . Theoretical studies on the MHD equilibrium of a four-fold advanced helical device [41] have demonstrated that the energy of periodicity-breaking perturbed configurations can be found in local minima with respect to the perturbation parameter. These minima lie below the energy of the unperturbed configurations and provide a natural explanation for the ease with which periodicity-breaking MHD modes can be found in real experiments.

- Investigation of the radial propagation of small, spontaneously generated, temperature perturbations using Transfer Entropy.

Electron heat transport in fusion plasmas presents significant challenges, among which one may consider extraordinary phenomena such as power degradation, rapid (non-local) transport, and profile stiffness. To study heat transport, we make use of a novel analysis technique, Transfer Entropy (TE), which measures the causal relation or information flow between two time series. This technique has some remarkable properties that converts it into a very sensitive tool to study the propagation of small perturbations in highly non-linear systems, such as fusion plasmas. TE has been firstly validated by analysing the propagation of heat waves in modulated ECRH TJ-II discharges and comparing with traditional Fourier techniques [42].

Then, we have applied it to analyse the propagation of small, spontaneously arising temperature perturbations in non-modulated discharges [43]. We show that heat transport in TJ-II is not a smooth and continuous (diffusive) process, but involves mini-transport barriers associated with low-order rational surfaces and rapid non-local radial 'jumps'. In addition, we find that the non-local contribution to transport becomes more prominent at higher input power, see Fig. 8. This remarkable finding might shed new light on the nature of anomalous transport.

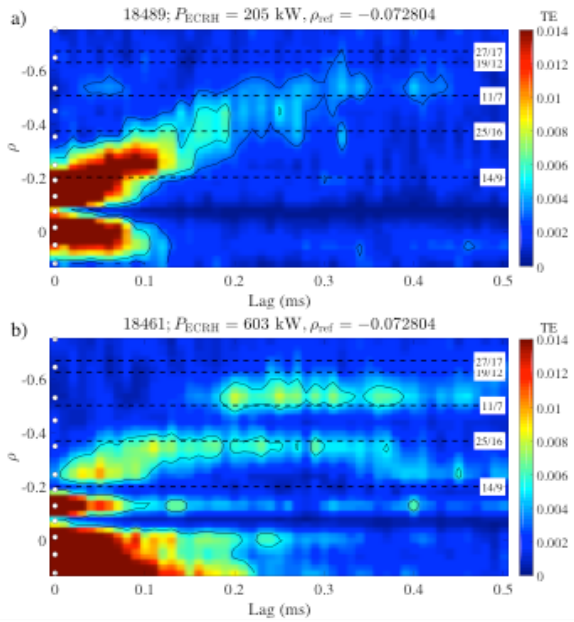

FIG. 8: Examples of Transfer Entropy, calculated from ECE data, between a reference channel and the others whose location is indicated by white circles at the left vertical axis. The reference ECE channel is located at $\rho_{ref} \approx -0.07$. Results for two heating powers are shown: a) $P_{ECRH} = 205kW$ and b) $P_{ECRH} = 603kW$. The color scale indicates the value of T. The approximate location of some major rational surfaces is indicated by horizontal dashed lines; the line labels specify the corresponding rotational transform, n/m.

6. PLASMA CORE FUELLING. PELLET PHYSICS AND MODELLING

Core fuelling is a critical issue on the pathway to the development of steady-state operational scenarios in magnetic confined plasmas. Cryogenic pellet injection (PI) has become a prime candidate for this purpose [44]. A compact pipe-gun type PI has been operated on TJ-II since 2014. Four different pellets can be injected at velocities between 800 and 1200 m/s into the plasma from its outer edge [45]. In dedicated experiments it was determined that pellet fuelling efficiency (pellet particles deposited in the plasma/number of pellet particles) in TJ-II can range from about $\sim 20\%$ to $\sim 80\%$, this value depending strongly on the pellet penetration depth [19]. Efficiencies tend to be $< 40\%$ for ECRH plasmas in which pellets do not penetrate beyond the magnetic axis. In contrast, for NBI heated plasmas, in which the core electron temperature is lower (300-400 eV), the fuelling efficiency is significantly higher. This tendency for increasing efficiency with penetration depth beyond the magnetic axis is considered to be due to inwards effective drifting of the partially ionized clouds that surround a pellet (plasmoids) created beyond that point. This has been understood from pellet ablation and deposition simulations made using a TJ-II adapted version of the Hydrogen Pellet Injection 2 code (HPI2) [46] (see figures 19 and 20 therein). Moreover, another study carried on TJ-II has shown that even when pellet particle density peaking is initially observed outside the core, this can be followed by an inward shift of the same [18]. Although pellet injections cannot be performed from the inner plasma edge on TJ-II (equivalent to high-field side injections in tokamaks) these studies indicate that a beneficial inwards drifting of pellet plasmoids may be present in

this device.

With the expansion of the TJ-II pellet database it has been observed that pellet fuelling efficiency can benefit from the presence of a population of fast electrons in its plasma core [47]. For instance, for ECRH plasmas, it has been determined that when no fast electrons are detected (by hard X-ray emissions or by excess pellet ablation), this efficiency is typically well below 30%. However, when a fast-electron population exists in the core when an injection is made (i.e., inside $\rho = 0.4$), then pellet penetration is truncated and fuelling increase by up to 50% [47]. Simulations of post-injection electron density profiles made with the TJ-II HPI2 code are in good agreement with Thomson Scattering density profiles for the former case. However, there are significant discrepancies between the simulated and experimental density profiles for latter case as the current TJ-II version of HPI2 code does not consider fast-electron effects [46]. Although the physics behind this increase is unclear at present, it is considered that pellet vaporization due to an abrupt heating of the ice may lead to a disruption of the processes of neutral cloud and plasmoid expansion and drift that normally occur. Other hypotheses, such as fast electron impacts causing a rocket effect that results in pellet deflection, also need to be investigated. In order to check these hypotheses it will be necessary to obtain fast-frame camera images captured from different viewing positions using a multiple-branch coherent fibre bundle. This will allow comparisons of plasmoid evolution along the magnetic field lines, and subsequent drifting across field lines. Also, modifications need to be made to the TJ-II version of HPI2 code. For instance, implementation of functions that consider excess ablation due to fast electrons or drift velocity modifications for plasmoids born at plasma radii where fast electrons occur could be implemented in order to achieve satisfactory agreement between simulated and experimental profiles.

As discussed in section 2, the need to explore favourable operation scenarios capable of preventing impurity accumulation is critical [48]. One method for performing such studies is the Tracer-Encapsulated Solid-Pellet (TESPEL) technique in which a hollow polystyrene shell, $(-CH(C_6H_5)CH_2-)_n$, filled with a known quantity of a suitable tracer element, is injected into a plasma [49]. In consequence, the impurity element is deposited directly in the plasma core, thereby eliminating inward diffusion from the physics.

Recently, a TESPEL injector was temporarily piggy-backed onto the up-stream end of PI [50, 51], thereby making it a unique system as both pellet types can be injected along adjoining guide tubes into the same toroidal sector of TJ-II, albeit not simultaneously. Although the *raison d'être* of both pellet injection methods is distinct, both types should undergo the same, or similar, physical processes as they travel through the plasma towards its core. Indeed, for both pellet types, the ablated particles in the plasmoid should experience the same physical effect(s) thus they should undergo similar processes, e.g., drift and diffusion. However, few systematic comparisons of these pellet types exist due to the limited number of devices equipped with both cryogenic and impurity pellet injection systems.

In a comparative study, it was shown that the post-injection electron density increase, after an injection in ECRH plasma, is significantly higher for carbon/hydrogen pellets that for solid hydrogen pellets (having similar electron content), as shown in Fig. 9. This is due to a reduction in plasmoid outwards drift for the former that is inversely proportional to particle atomic mass [52]. Although it is considered that pellet cloud pressure will be higher for hydrogen pellets, this is not sufficient to offset the higher carbon mass contribution.

Although it was reported in [53] that excess ablation was observed after penetration

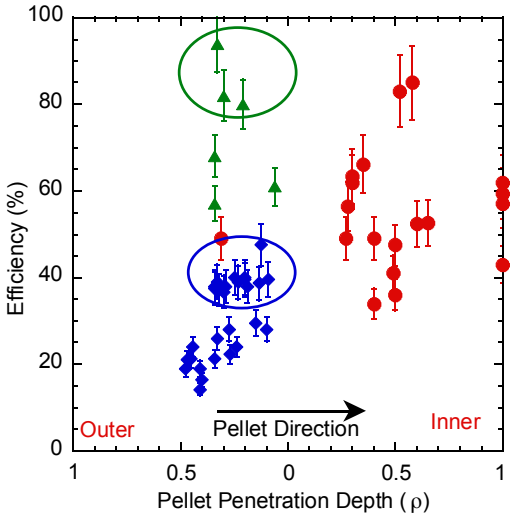

FIG. 9: Fuelling/deposition efficiency as a function of pellet penetration depth into TJ-II standard configuration plasmas. The data are for cryogenic hydrogen (filled blue diamonds) and polystyrene (green triangles) pellets injected into ECRH plasmas and cryogenic hydrogen pellets (red dots) injected into NBI plasmas. Cases for which a population of fast electrons is present in the core during pellet injection are contained within the ovals. Examples of pellets that are not fully ablated within the plasma are plotted on the right axis.

inside $\rho = 0.4$ for TESPEL, the enhancement of deposition efficiency due to fast electrons was not appreciated. However, when additional TESPEL data were considered, such an enhancement also occurs. Simulation of the TESPEL pellet injections using the TJ-II version of the HPI2 code will be complicated as the processes of polystyrene sublimation, carbon ionization, etc. need to be considered. Nonetheless, it is intended to continue with TESPEL injections into TJ-II plasmas and record images of the ablation and drift processes with the fast-camera system. It is hoped that this will help shed new light on pellet ablation physics.

7. CONTROL OF FAST PARTICLE DRIVEN MHD MODES

Experiments have been carried out in TJ–II NBI plasmas using ECRH on-axis with and without ECCD, in order to study the influence of Electron Cyclotron Current Drive (ECCD) on the observed Alfvén Eigenmodes (AEs) activity [54]. As shown in Fig. 10, a small amount of on-axis EECD, just -0.7 kA, has a strong impact on the observed Alfvénic activity: a steady mode in amplitude and frequency shows up.

To understand the changes measured in the AEs spectrum, the influence of the different contributions to the plasma current (NBCD, ECCD, Bootstrap) on the rotational transform profile has been calculated on the basis of the measured plasma profiles. Then, the resulting rotational transform profile is computed and used to obtain the Shear Alfvén Spectrum (SAS) by means of the STELLGAP [55]. The result indicates that the experimentally observed steady frequency mode could correspond to modes appearing in the $HAE_{2,1}$ gap. This gap becomes wider as the iota profile evolves from the pure NBI to the NBI+ECCD case, thus favouring the presence of the mode in the latter case.

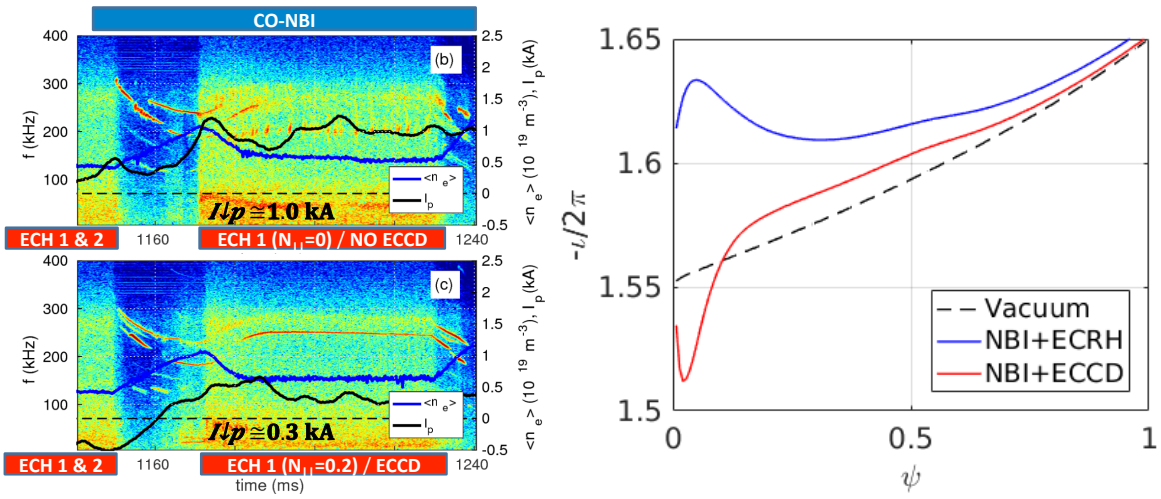

FIG. 10: Left: Spectrograms of magnetic fluctuations measured with a Mirnov coil for two plasma discharges with (upper box) and without (lower box) on-axis ECCD. Time traces of line average density (blue) and measured plasma current (black) are superimposed on both spectrograms. Right: Modelled iota profiles corresponding to the two discharges on the left: Blue and red color correspond to the cases without and with ECCD, respectively. Dashed line represents the vacuum iota profile

8. ALTERNATIVE PLASMA FACING COMPONENTS BASED ON LIQUID METALS

Two liquid metals (LM), Li and LiSn, presently considered as alternative materials for the divertor target of a fusion reactor, have been exposed to the plasma in a capillary porous system (CPS) arrangement in TJ-II [56] . A negligible perturbation of the plasma has been recorded in both cases, even when stellarator plasmas are particularly sensitive to high Z elements due to the tendency to central impurity accumulation. The surface temperature of the LM CPS samples (made of a tungsten mesh impregnated in SnLi or Li) has been measured during the plasma pulse with ms resolution by pyrometry and the thermal balance during heating and cooling has been used to obtain the thermal parameters of the SnLi and Li CPS arrangements, see Fig. 11. Temperatures as high as 1150 K during TJ-II plasma exposure were observed for the LiSn solid case. Strong changes in the thermal conductivity of the alloy were recorded in the cooling phase at temperatures close to the nominal melting point. The deduced values for the thermal conductivity of the LiSn alloy/CPS sample were significantly lower than those predicted from their individual components.

With respect to the potential use of LiSn alloys as LM for an alternative target in DEMO, the results obtained in TJ-II agree with the expectations from laboratory results, namely a dominant Li emission from the alloy when exposed to the plasma, in spite of its minority in its composition. Together with the very low H retention reported previously [57], the use of this alloy can be considered in a reactor. However, it must be pointed out that, in comparison with Li and Sn, the information about this alternative LM alloy is rather scarce. In particular, the low thermal conductivity inferred from the T versus t data and the possible depletion of Li from the alloy at long exposure times remain as potential showstoppers at present. More experimental work is required to fully validate

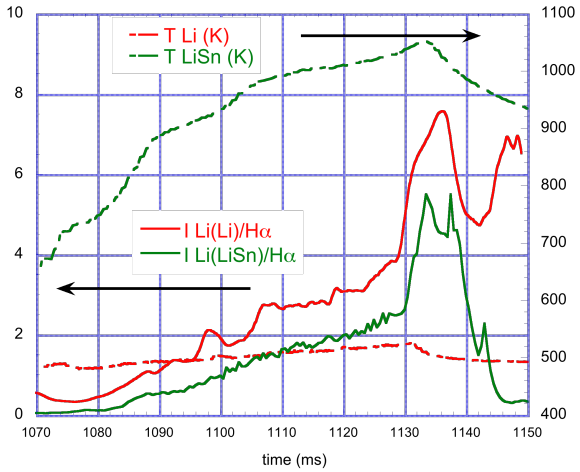

FIG. 11: Evolution of Li intensity for pure Li (red) and LiSn (green) samples during TJ-II plasma discharges (right vertical axis). The surface temperature evolution of the samples is also plotted (left vertical axis

this promising option.

ACKNOWLEDGMENTS

This work has been carried out within the framework of the EUROfusion Consortium and has received funding from the Euratom research and training programme 2014-2018 under grant agreement No 633053. The views and opinions expressed herein do not necessarily reflect those of the European Commission. It has been partially funded by the Ministerio de Ciencia, Inovación y Universidades of Spain under projects ENE2013-48109-P, ENE2015-70142-P and FIS2017-88892-P. It has also received funds from the Spanish Government via mobility grant PRX17/00425. The authors thankfully acknowledge the computer resources at MareNostrum and the technical support provided by the Barcelona S.C. It has been supported as well by The Science and Technology Center in Ukraine (STCU), Project P-507F

References

[1] K. McCormick et al., Phys. Rev. Lett. 89 (2002) 015001.
[2] K. Ida et al., Phys. Plasmas 16 (2009) 056111.
[3] J. M. García-Regaña et al., Nucl. Fusion 57, (2017) 056004.
[4] I. Calvo et al., Plasma Phys. Control. Fusion 59, (2017) 055014 .
[5] I. Calvo et al., J. Plasma Phys. 84, (2018) 905840407.
[6] J. L. Velasco et al., Plasma Phys. Control. Fusion 60, 0(2018) 74004 .
[7] A. Dinklage et al., Nucl. Fusion 53, (2013) 063022.
[8] J. L. Velasco et al., Nucl. Fusion 57 (2017) 57016016
[9] Y. Takeiri et al., Nucl. Fusion (2017) 102023.
[10] P. Helander et al., Phys. Rev. Lett. 118, 155002 (2017).
[11] I. Calvo et al., Nucl. Fusion 58 (2018) 124005.
[12] J. M. García-Regaña et al., PPCF, accepted (2018): arXiv:1804.10424.

[13] A. Mollén et al., Plasma Phys. Control. Fusion 60 084001 (2018).
[14] P. Monreal et al., Plasma Phys. Control. Fusion 5 9, 065005 (2017).
[15] A. Mishchenko, P. Helander, and A. Könies 2008 *Phys. Plasmas* 15 72309
[16] F. Jenko et al. 2000 *Phys. Plasmas* **7** 1904
[17] G. Jost et al. Physics of Plasmas, 8(7), 3321 (2001).
[18] J.L. Velasco et al. 2016 *Plasma Phys. Control. Fusion* 58 084004
[19] K. J. McCarthy et al., 2017 *Nuclear Fusion* 57 056039
[20] J.A. Alonso et al. Phys. Rev. Lett. 118.18, p. 185002 (2017).
[21] E. Sánchez, Plasma Phys. Control. Fusion 60 (2018) 094003 .
[22] E. Sánchez et al., "Validation of global gyrokinetic simulations in stellarator configurations " (this Conference, EX/P1-11).
[23] T. Estrada et al., "Turbulence and radial electric field asymmetries measured at TJ-II plasmas" (this Conference, EX/P1-9).
[24] M. Valovic et al Nucl. Fusion 48 (2008) 075006
[25] P. Vincenzi et al., Nuclear Fusion 55 (2015)113028
[26] L. Garzotti et al., Plasma Phys. Control. Fusion 56 (2014) 035004
[27] C. Angioni et al., Nucl. Fusion 57 (2017) 116053
[28] R. Sharma et al., Proc. 45th EPS Conference on Plasma Physics, Prague, Czech Republic 2018, Europhysics Conference Abstracts vol. 42A,P5.1061.
[29] R. Sharma, Ph. Khavanov et al., to be published.
[30] E. Sánchez et al., to be published.
[31] E. de la Cal, Nucl. Fusion 56 (2016) 106031.
[32] F. C. Prasanth, B. van Milligen et al., to be submitted.
[33] U. Losada et al., Plasma Phys. Control. Fusion 60 (2018) 074002.
[34] X. Garbet et al., Nucl. Fusion 34 (1994) 963.
[35] N. Mattor et al., Phys. Rev. Lett. 72 (1994) 486.
[36] W. X. Wang et al., Physics of Plasmas 14 (2007) 072306
[37] P. Beyer et al., Phys. Rev. Lett. 85 (2000) 4892
[38] G. Grenfell at al., "Measurement and control of turbulence spreading in the Scrape-Off Layer of TJ-II, accepted for publication in Nuclear Fusion.
[39] A. Alonso et al., Nuclear Fusion 52 (2012) 063010
[40] D. López-Bruna et al.,Nucl. Fusion 58 (2018) 106031
[41] A. W. Cooper et al., Nucl. Fusion 58 (to be published)
[42] B.Ph. van Milligen, et al., Nucl. Fusion 57, 5 (2017) 056028
[43] B. van Milligen et al., Phys. Plasmas 25 (2018) 062503.
[44] S. K. Combs and L. R. Baylor, Fusion Sci Tech. 73 (2018) 493.
[45] S. K. Combs et al., Fusion Sci Tech. 64 (2013) 513.
[46] N. Panadero et al., Nucl. Fusion 58 (2018) 026025.
[47] K. J. McCarthy et al., Plasma Phys. Control. Fusion 61(2019) 014013.
[48] R. Burhenn et al., Nucl. Fusion 49 (2009) 065005.
[49] S. Sudo et al., Rev. Sci. Instrum. 83 (2012) 023503

[50] N. Tamura et al., Rev. Sci. Instrum. 87 (2016) 11D619.

[51] K. J. McCarthy et al., Phys. Scripta 93 (2018) 035601.

[52] A. Matsuyama et al., Plasma Fusion Res: Lett. 7 (2012) 1303006.

[53] K. J. McCarthy et al., Europhys. Lett. 120 (2017) 25001.

[54] A. Cappa et al., Proc. 45th EPS Conference on Plasma Physics, Prague, Czech Republic 2018, Europhysics Conference Abstracts vol. 42A, P4.1040.

[55] D. Spong, R.Sánchez and A.Weller, Phys.of Plamas 10, 3217 (2003)

[56] F.L. Tabarés et al., 2017 Phys. Scr. 2017 014054

[57] F.L. Tabares F L et al 2016 Nucl. Mater. Energy 12 1368–73